Adaptive Multiple-Frame Image Super-Resolution Based on U-Curve

Qiangqiang Yuan, Liangpei Zhang, Huanfeng Shen, and Pingxiang Li

***Abstract*—Image super-resolution (SR) reconstruction has been a hot research topic in recent years. This technique allows the recovery of a high-resolution (HR) image from several low-resolution (LR) images that are noisy, blurred and down-sampled. Among the available reconstruction frameworks, the maximum *a posteriori* (MAP) model is widely used. In this model, the regularization parameter plays an important role. If the parameter is too small, the noise will not be effectively restrained; conversely, the reconstruction result will become blurry. Therefore, how to adaptively select the optimal regularization parameter has been widely discussed. In this paper, we propose an adaptive MAP reconstruction method based upon a U-curve. To determine the regularization parameter, a U-curve function is first constructed using the data fidelity term and prior term, and then the left maximum curvature point of the curve is regarded as the optimal parameter. The proposed algorithm is tested on both simulated and actual data. Experimental results show the effectiveness and robustness of this method, both in its visual effects and in quantitative terms.**

***Index Terms*—L-curve, regularization, super-resolution (SR) reconstruction, U-curve.**

I. Introduction

HIGH-RESOLUTION (HR) images are widely used in many fields, such as medical imaging [1], satellite imaging [2], and video surveillance [3]. However, because of the limitations of hardware, we obtain more low-resolution (LR) images than HR images. Consequently, researchers have explored new techniques to produce HR images from one or multiple frames of LR imagery, a technique that is called super-res olution (SR) technology.

The multiple-frame SR problem was first tackled by Tsai and Huang [4] in the frequency domain. Following their work, many frequency domain methods were developed. For example, Kim *et al.* [5], [6] improved Tsai and Huang's method by considering observation noise and spatial blurring. Bose *et al.* [7] proposed a recursive total least squares method for SR reconstruction to reduce effects of registration errors. A discrete cosine transform (DCT) based method was proposed by Rhee and Kang [8]. Wavelet transform-based [9]–[12] SR methods have also been proposed. However, although frequency domain methods are computationally attractive, they have some limitations. For example, it is difficult to incorporate the prior information about HR images using frequency domain methods. Therefore, many spatial domain methods have been successfully developed, including nonuniform interpolation approaches [13], [14], the iterative back projection (IBP) approach [15], [16], projection onto convex sets (POCS) approach [17], [18], deterministic regularized approach [19], maximum likelihood (ML) approach [20], [25], maximum *a posteriori* (MAP) approach [21], joint MAP approach [22]–[24], and hybrid approach [25]. Recently, based upon the reconstruction model mentioned previously, the SR technique has been extended to color or multiple-spectral image reconstruction [26]–[29].

This paper is mainly based upon the MAP reconstruction model. The regularization parameter plays a very important role in this model, controlling the tradeoff between the fidelity and prior item. In many implementations, the regularization parameter is selected manually, using a sequence of regularization parameters and selecting the parameter corresponding to the best results as the optimal one. However, this method is usually time-consuming and subjective. To avoid these disadvantages, some adaptive selection methods have been widely discussed in recent years. These methods can be divided into two groups. One group uses classical methods developed in the inverse problem field. For example, Bose *et al.* [30] use the L-curve method, which was introduced by Lawson and Hanson [31] and popularized by Hansen and O'Leary [32]. Nguyen *et al.* [33] use the generalized cross validation method (GCV) [34]. The second group use the general Bayesian framework to estimate parameters and reconstruct HR images simultaneously, obtaining parameters as well as the HR frame in each iteration step. This direction refers to the work of Kang and Katsaggelos [35], He and Kondi [36], Molina *et al.* [37] and Zibetti *et al.* [38]. The L-curve and GCV approaches can provide good solutions, but their computational costs are high. The Bayesian framework method has a lower computational load, but the optimal reconstruction result is more reliable on some attached parameters and parameter distribution functions, so it cannot be fully adaptive.

The U-curve method was first proposed by Krawczy-Stando and Rudnicki [39] to select the regularization parameter in inverse problems. It has been proved that the U-curve method not

Manuscript received May 15, 2009; revised December 17, 2009 and May 04, 2010; accepted June 09, 2010. Date of publication July 08, 2010; date of current version November 17, 2010. This work was supported in part by the Major State Basic Research Development Program (973 Program) of China under Grant 2009CB723905, by the National Natural Science Foundation of China under Grants 40930532, 40771139, 40801182, and 40971220, by the 863 High Technology Program of the People's Republic of China under Grant 2009AA12Z114, by the Program for New Century Excellent Talents in University under Grant NECT-10-0624, and by the Ph.D. research fund of Wuhan University. The associate editor coordinating the review of this manuscript and approving it for publication was Prof. Sabine Susstrunk.

Q. Yuan, L. Zhang, and P. Li are with the State Key Laboratory of Information Engineering in Surveying, Mapping, and Remote Sensing, Wuhan University, Wuhan 430072, China (e-mail: yqiang86@gmail.com; zlp62@public.wh.hb.cn; pxli@lmars.whu.edu.cn).

H. Shen is with the School of Resource and Environmental Science, Wuhan University, Wuhan 430072,China (e-mail: shenhf@whu.edu.cn).

Digital Object Identifier 10.1109/TIP.2010.2055571

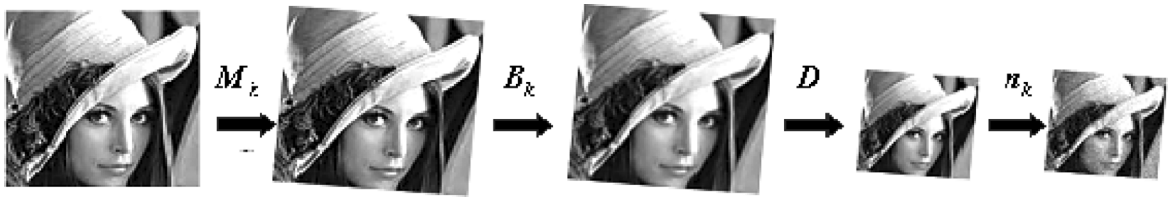

Fig. 1. Degradation model of the HR image.

only performed better than the L-curve, but also provides an interval where the optimal regularization parameter exists, which can reduce the computation load in searching for the optimal regularization parameter. However, in their work, the U-curve was just tested on some simple ill-posed problems. As a consequence, it is valuable and promising to develop the U-curve method in ill-posed problems included in the field of image processing, such as image restoration, SR, and so on. As the SR problem is a more complex inverse and ill-posed problem, the regularization model is more variable. Therefore, for the first time, we have applied the U-curve method on the MAP based SR model with Laplacian prior regularization, with the purpose of selecting the optimal regularization parameter adaptively, accurately, and efficiently.

The outline of this paper is as follows. The observation model is described in Section II. The MAP reconstruction model is given in Section III. The principle and the steps to select the optimal regularization parameter in the MAP model are detailed in Section IV. Experimental results and analyses are presented in Section V. Finally, conclusions are drawn in Section VI.

II. Observation Model

In this section, we describe the degradation process from an HR image to a LR image, which is also called the observation model.

Let the original HR image be denoted in vector form by $\boldsymbol{x} = [x_1\ x_2 \dots x_{l_1N_1 * l_2N_2}]$, where $l_1N_1 * l_2N_2$ is the size of the HR image. Assume that the HR image is subpixel shifted, blurred, down-sampled, and has some additive noise (Fig. 1), producing a sequence of LR images. Each frame of a sequence could be denoted in the vector form by $\boldsymbol{y}_k = [y_1 y_2 \dots y_{N_1 * N_2}]$, where $N_1 * N_2$ is the size of the LR image. $k = 1, 2 \dots k \dots p$. The observation model can be represented as

$$\boldsymbol{y}_k = \boldsymbol{D}_k\boldsymbol{B}_k\boldsymbol{M}_k\boldsymbol{x} + \boldsymbol{n}_k \tag{1}$$

Let l_1 and l_2 be the down-sampled factors for rows and columns, respectively, $\boldsymbol{M}_k$ stands for the warp matrix with size $l_1N_1l_2N_2 * l_1N_1l_2N_2$, $\boldsymbol{B}_k$ is the blurring matrix (PSF) with size $l_1N_1l_2N_2 * l_1N_1l_2N_2$, $\boldsymbol{D}_k$ is the down-sampling matrix with size $N_1N_2 * l_1N_1l_2N_2$. $\boldsymbol{n}_k$ is the noise vector with size MN. In this paper, we assume that the down-sample factors and blurring function remain the same between the LR images, so the matrices $\boldsymbol{D}_k$ and $\boldsymbol{B}_k$ will be substituted by matrices $\boldsymbol{D}$ and $\boldsymbol{B}$, respectively, in the remaining parts of the paper.

Each LR image has an observation model in the form of function (1). If we incorporate them, the whole observation model could be represented as

$$\left.\begin{aligned} \boldsymbol{y}_1 &= \boldsymbol{D}BM_1\boldsymbol{x} + \boldsymbol{n}_1 \\ \boldsymbol{y}_2 &= \boldsymbol{D}BM_2\boldsymbol{x} + \boldsymbol{n}_2 \\ &\vdots \\ \boldsymbol{y}_p &= \boldsymbol{D}BM_p\boldsymbol{x} + \boldsymbol{n}_p \end{aligned}\right\} \rightarrow \boldsymbol{y} = \boldsymbol{D}BMx + \boldsymbol{n} \tag{2}$$

where $\boldsymbol{y} = [\boldsymbol{y}_1, \boldsymbol{y}_2 \dots \boldsymbol{y}_p]^T, \boldsymbol{M} = [\boldsymbol{M}_1, \boldsymbol{M}_2 \dots \boldsymbol{M}_p]^T$ and $\boldsymbol{n} = [\boldsymbol{n}_1, \boldsymbol{n}_2 \dots \boldsymbol{n}_p]^{\boldsymbol{T}}$.

III. MAP Reconstruction Model

As SR is an ill-posed problem, we cannot solve the HR image from the observation model directly. Therefore, a MAP model is used to add some prior information about the HR image to regularize the SR problem.

In this section, we discuss the formulation of the reconstruction function using the MAP model and how to solve it.

A. MAP Reconstruction Model

For the MAP model, given the LR images, the HR image can be estimated as

$$\hat{\boldsymbol{x}} = \arg\max\{p(\boldsymbol{x} \,|\, \boldsymbol{y})\}. \tag{3}$$

Using Bayes rule, function (3) can alternatively be expressed as

$$\hat{\boldsymbol{x}} = \arg\max\left\{\frac{p(\boldsymbol{y} \,|\, \boldsymbol{x})p(\boldsymbol{x})}{p(\boldsymbol{y})}\right\}. \tag{4}$$

Because the estimated HR image is independent of $p(\boldsymbol{y})$, function (4) can be written as

$$\hat{\boldsymbol{x}} = \arg\max\{p(\boldsymbol{y}_1 \dots \boldsymbol{y}_p \,|\, \boldsymbol{x})p(\boldsymbol{x})\} \tag{5}$$

where $p(\boldsymbol{y}_1 \dots \boldsymbol{y}_p \,|\, \boldsymbol{x})$ is the likelihood distribution of the LR images, and $p(\boldsymbol{x})$ is the prior distribution of the HR images. Since we later define the form of these densities of noise to be zero-mean Gaussian in nature, it is more convenient, and equivalent, to minimize the minus log of the functional in (8). This yields

$$\hat{\boldsymbol{x}} = \arg\min\{-(\log p(\boldsymbol{y}_1 \dots \boldsymbol{y}_p \,|\, \boldsymbol{x}) + \log p(\boldsymbol{x}))\}. \tag{6}$$

Assuming that the noise is zero-mean Gaussian noise and each LR frame is independent, $p(\boldsymbol{y}_1 \dots \boldsymbol{y}_p \,|\, \boldsymbol{x})$ can be written as

$$p(\boldsymbol{y}_1 \dots \boldsymbol{y}_p \,|\, \boldsymbol{x}) = \left(\frac{1}{\sqrt{2\pi}\sigma_k}\right)^p \times \exp\left(-\sum_{k=1}^{p} \frac{\|\boldsymbol{y}_k - \boldsymbol{D}B_k\boldsymbol{M}_k\boldsymbol{x}\|^2}{2\sigma_k^2}\right). \quad (7)$$

For the HR image, the following prior model is used in this paper:

$$p(\boldsymbol{x}) = \frac{1}{C}\exp\left\{-\frac{1}{\eta}\|\boldsymbol{Q}x\|^2\right\} \quad (8)$$

where η is a parameter that controls the variance of the prior distribution and $\boldsymbol{Q}$ represents a linear high-pass operation that penalizes the estimation that is not smooth. $\boldsymbol{Q}$ is chosen as a 2-D Laplacian matrix in this paper.

Substituting (7) and (8) in (6), the cost function can be written as

$$\hat{\boldsymbol{x}} = \arg\min J(\boldsymbol{x}) = \arg\min\{\|\boldsymbol{y} - \boldsymbol{D}BMx\|^2 + \alpha\|\boldsymbol{Q}x\|^2\}. \quad (9)$$

In function (9), $\|\boldsymbol{y} - \boldsymbol{D}BMx\|^2$ is the data fidelity item, which stands for the fidelity between the observed LR image and the original HR image, $\|\boldsymbol{Q}x\|^2$ is the prior item, which stands for the prior distribution of the HR image. α is the regularization parameter, which controls the tradeoff between the data fidelity and prior item.

B. Optimization

A gradient descent procedure is designed to minimize the cost function. Differentiating (9) with respect to $\boldsymbol{x}$, and setting the result equal to zero, we have

$$\nabla J(x) = -2\boldsymbol{M^T B^T D^T}(\boldsymbol{y} - \boldsymbol{D}BMx) + 2\alpha\boldsymbol{Q^T Q}x = 0. \quad (10)$$

The HR image is solved by employing the successive approximations iteration

$$\boldsymbol{x}^{n+1} = \boldsymbol{x}^n + \beta^n \boldsymbol{r}^n \quad (11)$$

where

$$\boldsymbol{r^n} = -\frac{1}{2}\nabla J(\boldsymbol{x}) = \boldsymbol{M}^T\boldsymbol{B}^T\boldsymbol{D}^T(\boldsymbol{y} - \boldsymbol{D}BMx) - \alpha\boldsymbol{Q^T Q}x \quad (12)$$

β^n stands for the nth iteration step size, which is critical for convergence. It has the form

$$\beta^n = \frac{(\boldsymbol{r}^n)^{\mathbf{T}}\boldsymbol{r}^n}{\|\boldsymbol{D}BMr^n\|^2 + \lambda\|\boldsymbol{Q}r^n\|^2}. \quad (13)$$

The iteration is terminated when

$$\frac{\|\boldsymbol{x}^{n+1} - \boldsymbol{x}^n\|^2}{\|\boldsymbol{x}^n\|^2} \le d. \quad (14)$$

IV. U-Curve Method

This section describes the novel approach to estimate the regularization parameter based upon the U-curve. First, we introduce the principle of the U-curve and its properties. Second, the use of the U-curve method in the SR problem is presented.

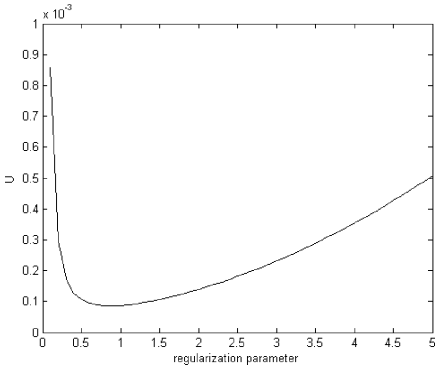

Fig. 2. Typical U-curve.

TABLE I
DISPLACEMENT PARAMETERS OF THE FOUR LR IMAGES

	Vertical (pixel)	Horizontal (pixel)
Image 1	0	0
Image 2	0.5	0.5
Image 3	0.5	0
Image 4	0	0.5

TABLE II
PSF AND NOISE PARAMETERS OF CASE 1 AND CASE 2

	PSF ([size, variance])	Noise ([mean, variance])
Case 1	[3,0.5^2]	(0,0.01^2)
Case 2	[5,1.0^2]	(0,0.02^2)

A. U-Curve and Its Properties

Because the Gaussian zero-mean noise model and Laplacian prior model are used, the MAP model proposed in this paper has an expression similar to the traditional Tikhonov regularization model. Therefore, the explanation of the principle of the U-curve is based upon the Tikhonov model.

Let matrix $\boldsymbol{A}$ stand for the degradation matrix $\boldsymbol{D}BM$. The cost function presented in (9) can be written like the traditional model of Tikhonov regularization as

$$\hat{\boldsymbol{x}} = \arg\min\{\|\boldsymbol{y} - \boldsymbol{A}x\|^2 + \alpha\|\boldsymbol{Q}x\|^2\}. \quad (15)$$

Using the singular value decomposition (SVD) least squares method, the regularized solution $\hat{\boldsymbol{x}}_{\boldsymbol{\alpha}}$ of function (15) is

$$\boldsymbol{A} = \boldsymbol{U}\begin{bmatrix}\sum & \mathbf{0}\\ \mathbf{0} & \mathbf{0}\end{bmatrix}\boldsymbol{V} \quad \boldsymbol{g} = \boldsymbol{U^T y}$$

$$\hat{\boldsymbol{x}}_{\boldsymbol{\alpha}} = \sum_{i=1}^{r}\frac{\sigma_i g_i \boldsymbol{v}_i}{(\sigma_i^2 + \alpha q_i^2)} \quad (16)$$

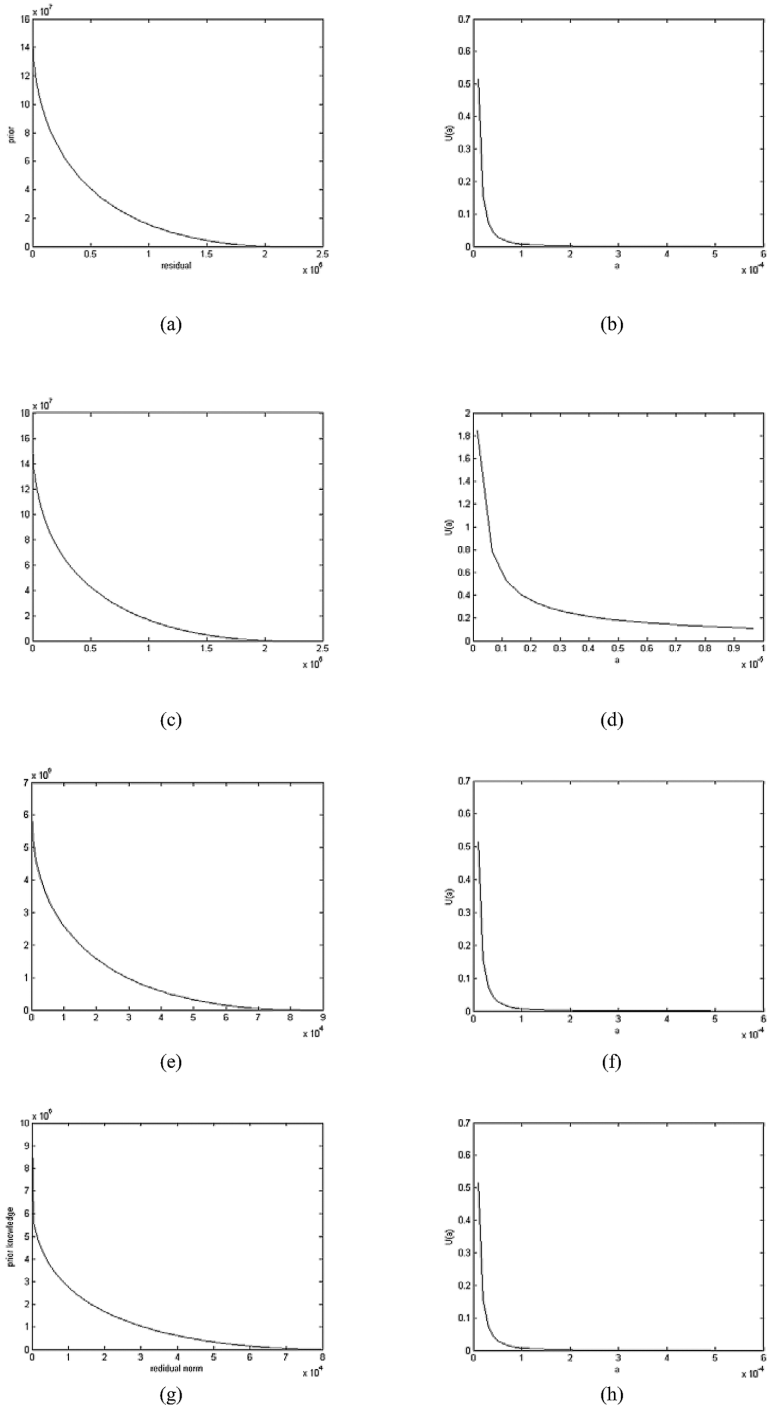

Fig. 3. L-curve, U-curve, and the selected regularization parameter of the "cameraman" image and "boat" image in Cases 1 and 2. (a) L-curve in Case 1 ($\alpha = 0.012$) (cameraman). (b) U-curve in Case 1 ($\alpha = 0.63e-4$) (cameraman). (c) L-curve in Case 2 ($\alpha = 0.015$) (cameraman). (d) U-curve in Case 2 ($\alpha = 0.13e-5$) (cameraman). (e) L-curve in Case 1 ($\alpha = 0.014$) (boat). (f) U-curve in Case 1 ($\alpha = 0.72e-4$) (boat). (g) L-curve in Case 2 ($\alpha = 0.021$) (boat). (h) U-curve in Case 2 ($\alpha = 0.78e-5$) (boat).

where $\boldsymbol{U}$ is the left SVD matrix of $\boldsymbol{A}, \boldsymbol{v}_i$ is the ith column of the right SVD matrix $\boldsymbol{V}$. σ_i is the singular values of $\boldsymbol{A}$, and $\sigma_r \leq \sigma_{r-1} \leq \cdots \leq \sigma_i \leq \cdots \sigma_1$. q_i is the ith singular value of $\boldsymbol{Q}$, and $q_r \leq q_{r-1} \leq \ldots \leq q_i \leq \ldots q_1$. g_i is the i th value of $\boldsymbol{g}$.

From functions (15) and (16), it is found that

$$R(\alpha) = \|\boldsymbol{y} - \boldsymbol{A}x\|^2 = \sum_{i=1}^{r} \frac{\alpha^2 q_i^4 g_i^2}{\left(\sigma_i^2 + \alpha q_i^2\right)^2} \tag{17}$$

$$P(\alpha) = \|\boldsymbol{Q}x\|^2 = \sum_{i=1}^{r} \frac{\sigma_i^2 q_i^2 g_i^2}{\left(\sigma_i^2 + \alpha q_i^2\right)^2}. \tag{18}$$

From the previous discussion, we define

$$U(\alpha) = \frac{1}{R(\alpha)} + \frac{1}{P(\alpha)}. \tag{19}$$

The U-curve is the plot of $U(\alpha)$. Fig. 2 shows a typical example of the U-curve.

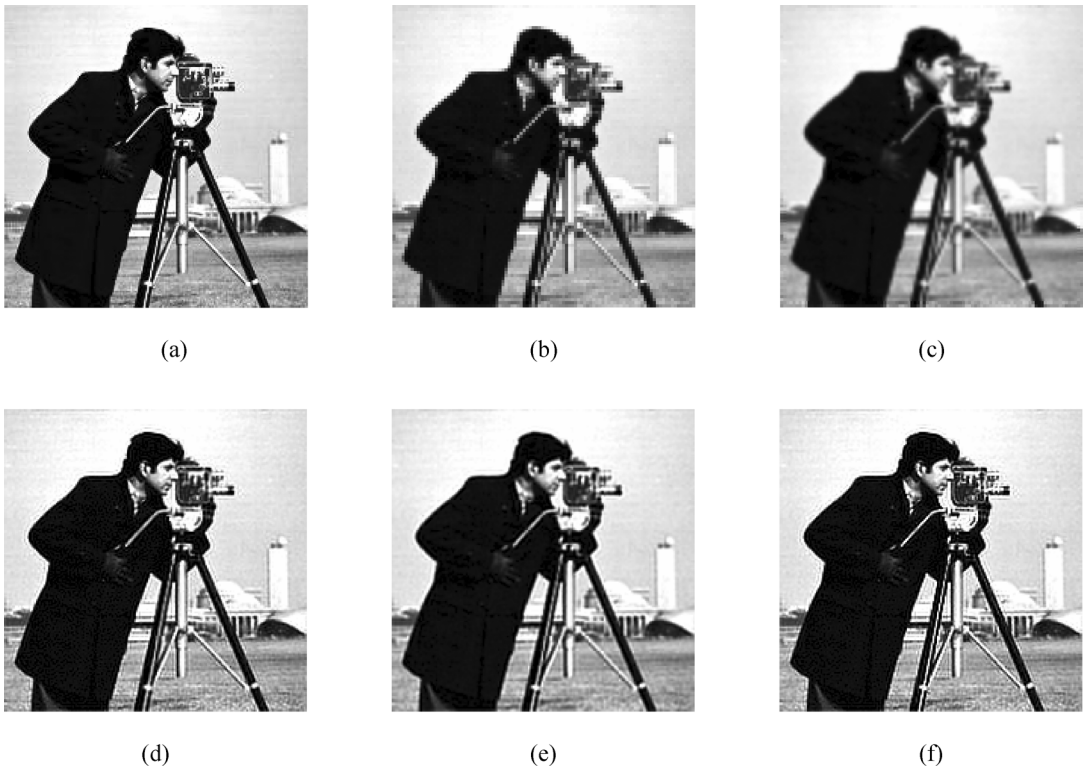

Fig. 4. Reconstruction results of the "cameraman" image in Case 1. (a) Original HR image. (b) LR image. (c) BI. (d) Adaptive iteration. (e) L-curve. (f) U-curve.

It is clearly seen from Fig. 2 that a U-curve has three characteristic parts: (a) it is monotonically decreasing on the left side; (b) it is monotonically increasing on the right side; (c) in the middle it is almost "horizontal" with monotonous change. The left and right sides correspond to the regularization parameter for which the data fidelity item and the prior item are dominated by each other. The more horizontal part corresponds to the regularization parameter for which the data fidelity item and the prior item are close to each other, and this part is where the optimal regularization parameter exists.

From the discussion in [39], the U-curve has the following properties:

a) for $\alpha \in (0, (\sigma_r/q_1)^{(4/3)})$, the function $U(\alpha)$ is strictly decreasing;
b) for $\alpha \in ((\sigma_1/q_r)^{(4/3)}, +\infty)$, the function $U(\alpha)$ is strictly increasing;
c) $\lim U(\alpha)_{\alpha \to 0^+} = +\infty$; and
d) $\lim U(\alpha)_{\alpha \to +\infty} = +\infty$.

From the previously mentioned properties, the following remark can be made:

Remark: The optimal regularization parameter can be selected in the interval $((\sigma_r/q_1)^{(4/3)}, (\sigma_1/q_r)^{(4/3)})$, and the objective of the U-curve criterion for selecting the regularization parameter is to choose a parameter for which the curvature of the U-curve attains a local maximum close to the left part of the U-curve.

B. Selection Steps

For the MAP reconstruction model presented in (9), we can use the U-curve method to determine the optimal regularization parameter α, and the selection steps can be expressed as follows.

Step 1) Singular value decomposition to the degradation matrix $\boldsymbol{A}$ and matrix $\boldsymbol{Q}$; record the singular values of $\boldsymbol{A}$ as $\sigma_r \leq \sigma_{r-1} \leq \cdots \leq \sigma_i \leq \cdots \sigma_1$; record the first r singular values $\boldsymbol{Q}$ as $q_r \leq q_{r-1} \leq \cdots \leq q_i \leq \ldots q_1$.

Step 2) Incorporate the result of Step 1 into function (17) and (18); construct $U(\alpha)$ from (19).

Step 3) Plot the U-curve in the interval $((\sigma_r/q_1)^{(4/3)}, (\sigma_1/q_r)^{(4/3)})$.

Step 4) Select the maximum curvature point close to the left vertical part of the U-curve as the optimal regularization parameter.

V. Experimental Results

We use the mean square error (MSE) and the structural similarity (SSIM) to evaluate the reconstruction results. The MSE is usually employed to evaluate the gray value similarity, and the SSIM proposed by Wang *et al.* [40] is used to evaluate the SSIM. Their expressions are as follows:

$$\text{MSE} = \frac{1}{l_1 N_1 * l_2 N_2} \|\hat{\boldsymbol{x}} - \boldsymbol{x}\|^2 \tag{20}$$

$$\text{SSIM} = \frac{(2\mu_x \mu_{\hat{x}} + C_1)(2\sigma_{x\hat{x}} + C_2)}{(\mu_x^2 + \mu_{\hat{x}}^2 + C_1)(\sigma_x^2 + \sigma_{\hat{x}}^2 + C_2)} \tag{21}$$

where $\boldsymbol{x}$ represents the original HR image, and $\hat{\boldsymbol{x}}$ represents the reconstructed HR image. $l_1 N_1 * l_2 N_2$ is the size of the HR image. μ_x and $\mu_{\hat{x}}$ represent the average gray value of the original HR and the reconstructed result, respectively. σ_x and $\sigma_{\hat{x}}$ represent the variance of the original HR image and the reconstructed image, respectively, $\sigma_{x\hat{x}}$ represents the covariance between the original HR image and the reconstructed image. C_1

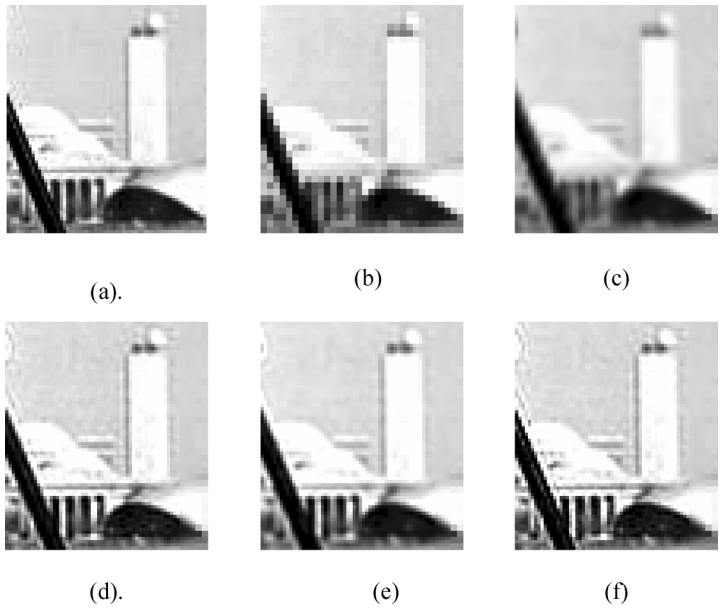

(a). (b) (c)

(d). (e) (f)

Fig. 5. Detailed regions cropped from Fig. 4. (a) Original HR image. (b) LR image. (c) BI. (d) Adaptive iteration. (e) L-curve. (f) U-curve.

and C_2 are two constants, which prevent unstable results when either $\mu_x^2 + \mu_{\hat{x}}^2$ or $\sigma_x^2 + \sigma_{\hat{x}}^2$ is very close to zero.

A. Simulated Data

Three simulated data sets were used to test the efficacy and robustness of the proposed method: the "cameraman" image of size $200*200$, the "boat" image of size $256*256$ and the "castle" image sequence which was obtained from LCAV(EPFL) [41], consisting of four subpixel displacement LR images with the size of $128 * 128$. The gray values of both data sets are between 0 and 255. The three simulated experiments were classified into two cases according to the degradation parameters were known or not. In the case of known degradation parameters, the original HR "cameraman" image and "boat" image were shifted with subpixel displacements to produce four LR images; the sequence was convoluted with Gaussian smooth filter PSF; then down-sampled in both the vertical and horizontal directions; lastly, zero-mean Gaussian-noise was added to the sequence. In these two experiments, the motion matrix and blur matrix were both constructed with the known degradation parameters; In the case of unknown degradation parameters, because the degradation parameters "castle" image sequence were not known, the displacement parameters were estimated using the well-performed registration approach presented in [43], and the degradation matrix was constructed with the estimated parameters.

Our results are compared with those of bilinear interpolation (BI), the bicubic interpolated (BCI). the adaptive iteration approach in [35] and the L-curve method in [30]. The reconstruction factor was selected as 2. The termination condition of the iteration was defined as

$$\frac{||\boldsymbol{x}^{n+1} - \boldsymbol{x}^n||^2}{||\boldsymbol{x}_n||^2} \leq \mathbf{10^{-6}}.$$

1) Degradation Parameters Known Case: For each image, we experimented with the proposed method in two different cases. The parameter values of Case 1 and Case 2 are shown in Tables I and II.

Case 1: the original HR image was shifted with subpixel displacements to produce four LR images; the sequence was convoluted with PSF of $3 * 3$ window size and 0.5 variance; then down-sampled with a factor 2 in both the vertical and horizontal directions; lastly, zero-mean Gaussian-noise with 0.01 variance was added to the sequence.

Case 2: the original HR image was shifted with the same subpixel displacements as in Case 1 to produce four LR images; the sequence was convoluted with a PSF of $5 * 5$ window size and 1.0 variance; then down-sampled with a factor 2 in both the vertical and horizontal directions; lastly, zero-mean Gaussian-noise with 0.02 variance was added to the sequence.

Fig. 3 shows the L-curve and the U-curve and the selected regularization parameters of the "cameraman" image and "boat" image. Because we just draw the U-curve between the interval $((\sigma_r/q_1)^{(4/3)}, (\sigma_1/q_r)^{(4/3)})$ where the optimal regularization parameter exits, the U-shape is not visible in Fig. 3. The reconstruction results of the "cameraman" and "boat" image in Case 1 are, respectively, shown in Figs. 4 and 7. To facilitate a better comparison, a region of each is shown in detail in Figs. 5 and 8. The quantitative comparison of the results using MSE and SSIM is shown in Tables III and IV. The difference between the result and the HR image is shown in Figs. 6 and 9.

From the comparison of the results, it can be clearly seen that the U-curve method provides a better result than other methods; it is closer to the original HR image and provides the lowest MSE value and the highest SSIM, which indicates that the U-curve method provides good representation of the original HR image, both in terms of gray values and structure. The bilinear interpolated (BI) result is the poorest, which confirms the promise of the SR technology. For the adaptive iteration method, the reconstruction result is more dependent

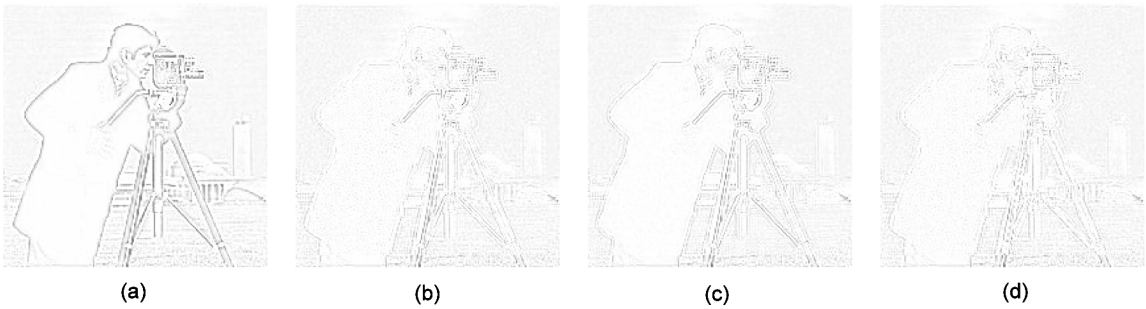

Fig. 6. Difference between the reconstruction results and the original image in Case 1. (a) BI. (b) Adaptive iteration. (c) L-curve. (d) U-curve.

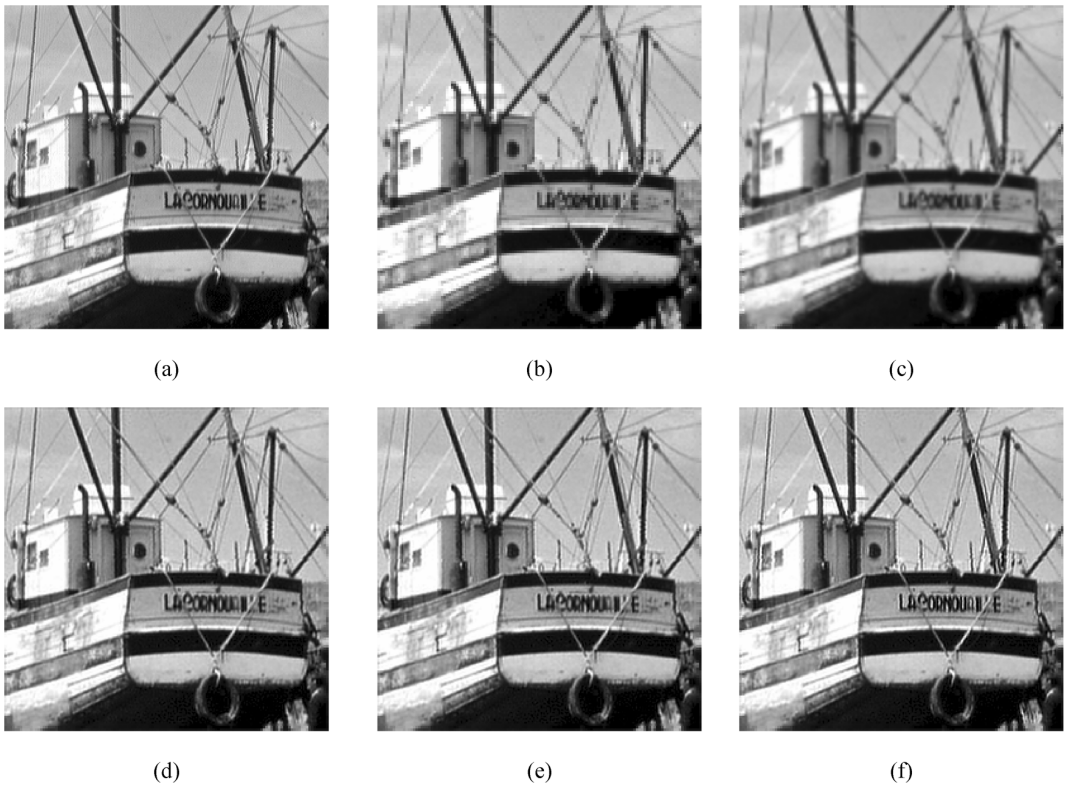

Fig. 7. Reconstruction results of the "boat" image in Case 1. (a) Original HR image. (b) LR image. (c) BI. (d) Adaptive iteration. (e) L-curve. (f) U-curve.

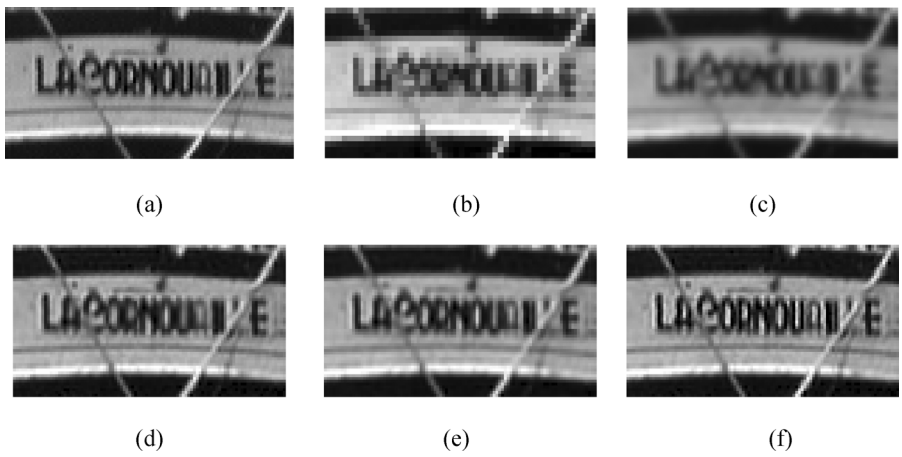

Fig. 8. Detailed regions cropped from Fig. 7. (a) Original HR image. (b) LR image. (c) BI. (d) Adaptive iteration. (e) L-curve. (f) U-curve.

(a) (b) (c) (d)

Fig. 9. Difference between the reconstruction results and the original image in Case 1. (a) BI. (b) Adaptive iteration. (c) L-curve. (d) U-curve.

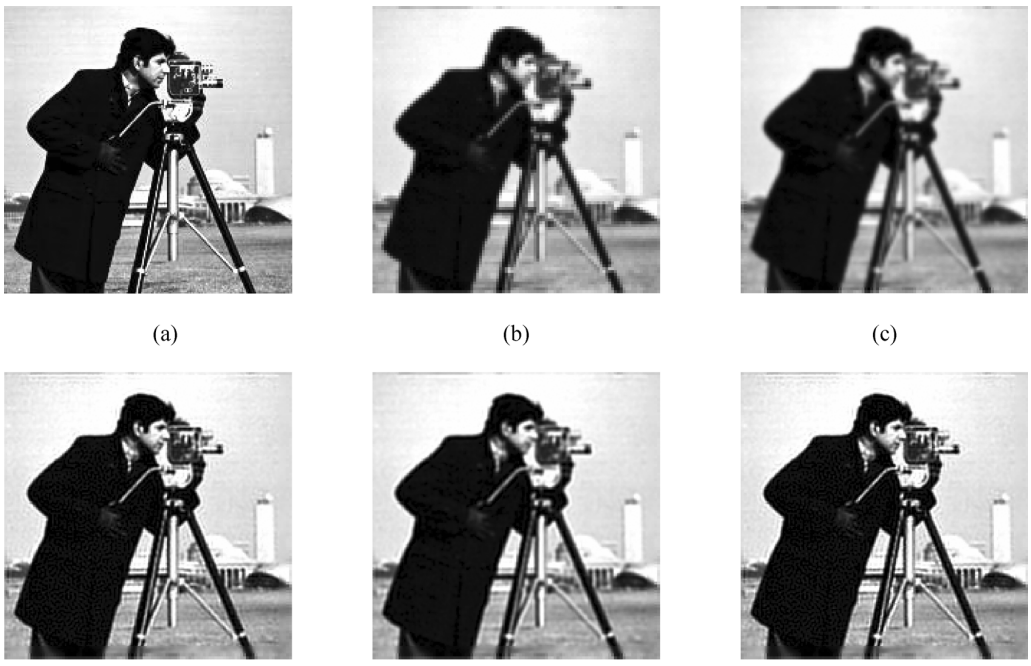

(a) (b) (c)

(d) (e) (f)

Fig. 10. Reconstruction results of the "cameraman" image in Case 2. (a) Original HR image. (b) LR image. (c) BI. (d) Adaptive iteration. (e) L-curve. (f) U-curve.

TABLE III
MSE AND SSIM VALUE OF DIFFERENT RECONSTRUCTION METHODS IN CASE 1 (CAMERAMAN)

	BI	Adaptive iteration	L-curve	**U-curve**
MSE	490.525	168.019	194.098	**149.995**
SSIM	0.82732	0.87471	0.85412	**0.88368**

TABLE IV
MSE AND SSIM VALUE OF DIFFERENT RECONSTRUCTION METHODS IN CASE 1 (BOAT)

	BI	Adaptive iteration	L-curve	**U-curve**
MSE	207.203	82.644	87.481	**76.900**
SSIM	0.81339	0.91393	0.90835	**0.91587**

upon the selection of the parameter γ. If we properly define the parameter γ, a result as good as our proposed method could be obtained. However, the selection of γ may require a large computational load, so this method cannot be fully adaptive. For the L-curve method, because the selected regularization parameter is larger, the reconstruction result became blurred, and some detailed information is lost.

To show the robustness of the proposed method, we plot the change of the MSE value under different SNR noise condition (SNR from 50 to 10 db). The results are shown in Fig. 14. It is clearly illustrated that the proposed method also remains robust when the degree of noise becomes higher. The reconstruction of the "cameraman" and "boat" images in Case 2 are shown in Figs. 10 and 12, respectively. Detailed regions of the reconstruction are shown in Figs. 11 and 13; the quantitative comparison is shown in Tables V and VI.

2) Degradation Parameters Unknown Case: The reconstruction results of the "castle" image sequence are shown in Fig. 15.

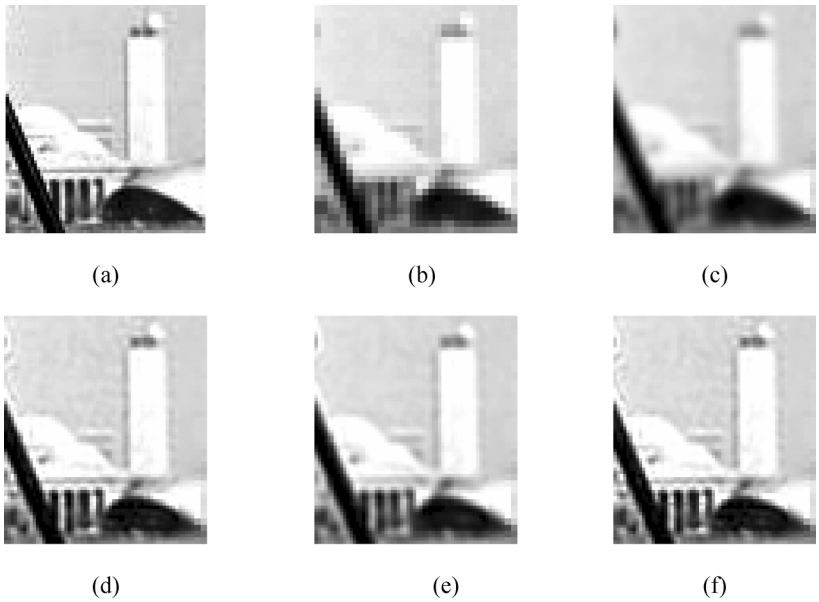

Fig. 11. Detailed regions cropped from Fig. 10. (a) Original HR image. (b) LR image. (c) BI. (d) Adaptive iteration. (e) L-curve. (f) U-curve.

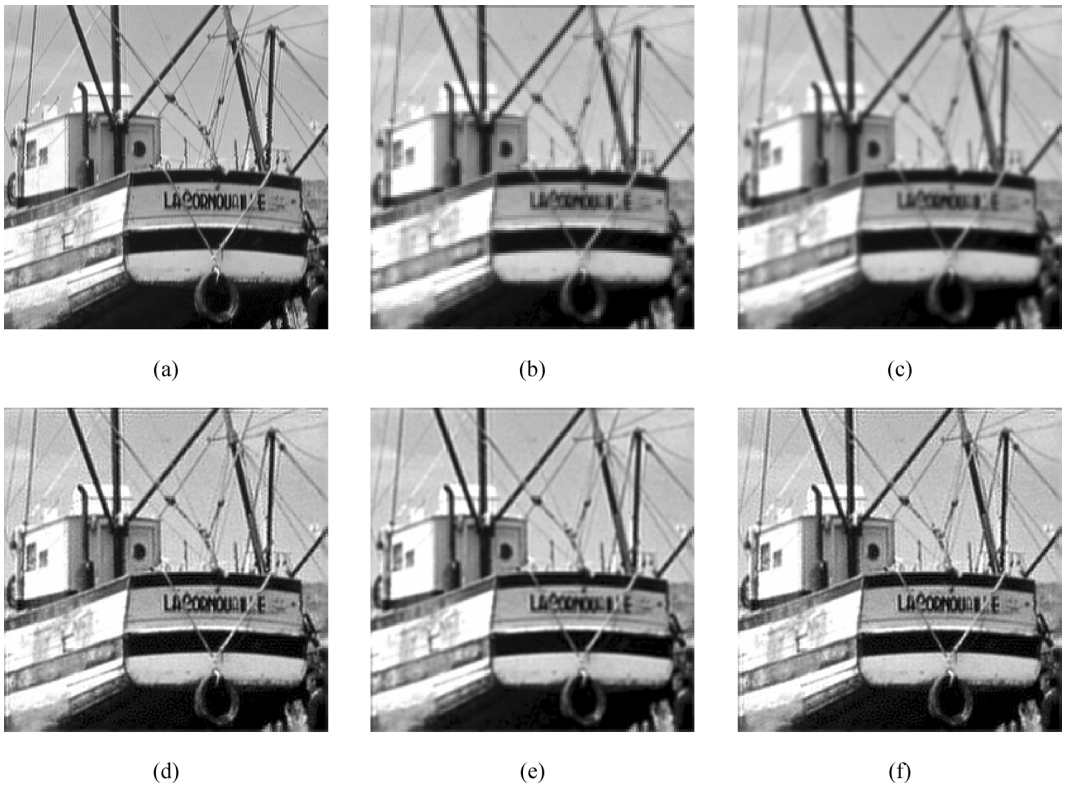

Fig. 12. Reconstruction results of the "boat" image in Case 2. (a) Original HR image. (b) LR image. (c) BI. (d) Adaptive iteration. (e) L-curve. (f) U-curve.

Fig. 15(a) shows one of the LR images; the BI and the BCI results are, respectively, shown in Fig. 15(b) and (c); Fig. 15(d) shows the result of the adaptive iterative method. Fig. 15(e) presents the result of the L-curve method, and Fig. 15(f) presents the result of the proposed method. The detailed regions cropped from Fig. 15(a)–(f) are, respectively, shown in Fig. 16(a)–(f).

From the comparison of the results, the SR images look better than the interpolated result. It can be seen that the U-curve reconstruction method provides a better result than other methods. The result presents more details than the L-curve; this effect is very obvious in the detailed regions. For the adaptive iteration method, although the result looks as good as the proposed method, as discussed previously we must adjust the parameter γ to obtain the best result, so it cannot be fully adaptive. Because the original HR image of the "castle" image sequence cannot be obtained, the reconstruction results cannot be evaluated with the MSE and SSIM indices.

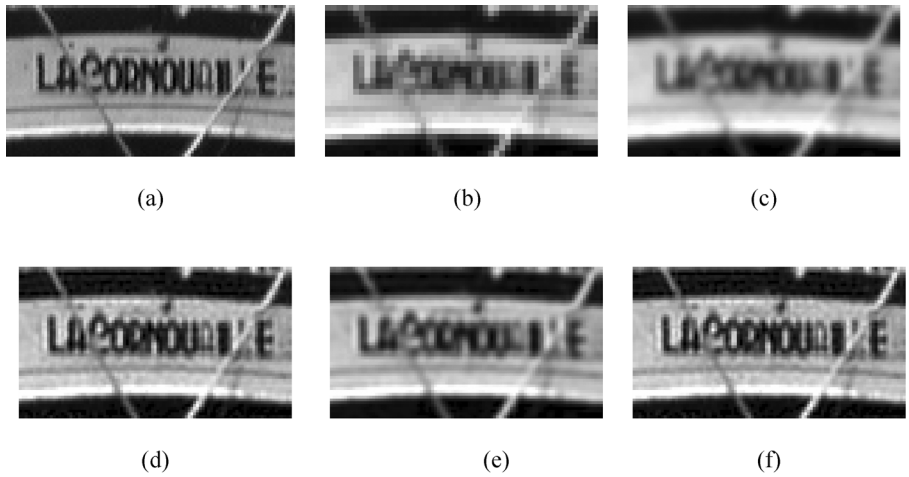

Fig. 13. Detained regions cropped from Fig. 12. (a) Original HR image. (b) LR image. (c) BI. (d) Adaptive iteration. (e) L-curve. (f) U-curve.

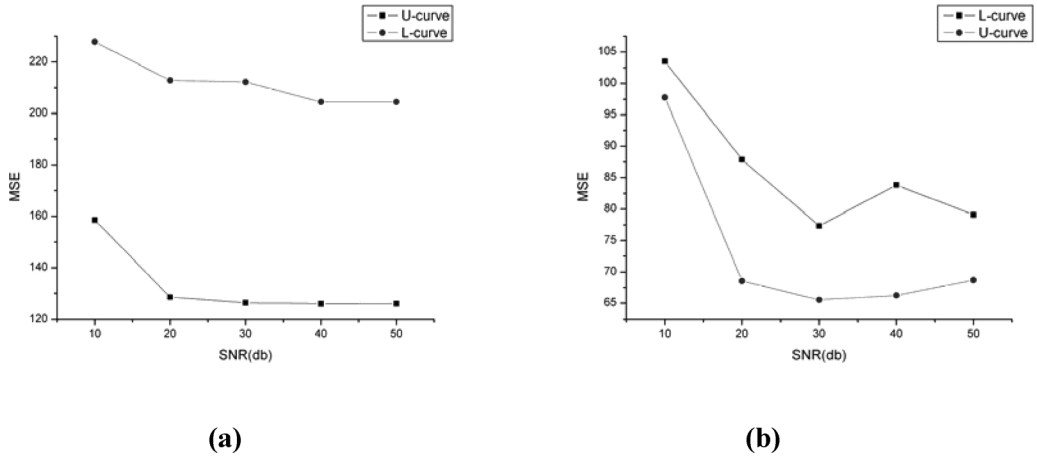

(a) **(b)**

Fig. 14. Reconstruction MSE value under different SNR noise. (a) Cameraman image. (b) Boat image.

TABLE V
MSE AND SSIM VALUE OF DIFFERENT RECONSTRUCTION METHODS IN CASE 2 (CAMERAMAN)

	BI	Adaptive iteration	L-curve	**U-curve**
MSE	628.625	258.083	370.885	**247.221**
SSIM	0.77178	0.81563	0.80262	**0.82223**

TABLE VI
MSE AND SSIM VALUE OF DIFFERENT RECONSTRUCTION METHODS IN CASE 2 (BOAT)

	BI	Adaptive iteration	L-curve	**U-curve**
MSE	296.904	135.262	174.338	**130.788**
SSIM	0.74568	0.84081	0.82704	**0.84935**

B. Real Data

To further illustrate the performance of the proposed method, we tested it on a real data sets. The real data "text" video sequence was obtained from the Multidimensional Signal Processing (MDSP) Research Group of UCSC [42], consisting of 30 frames with the size of $49*57$. In order to reduce the computational load, we just selected the first seven frames in our experiment. The well-performed registration approach presented in [43] was used as the motion estimation method.

Fig. 17(a) shows one of the LR frames of the video; the BI and the BCI results are, respectively, shown in Fig. 17(b) and (c); Fig. 17(d) shows the result of the adaptive iteration method; Fig. 17(e) illustrates the result of the L-curve method; and Fig. 17(f) presents the result of the proposed method. The detailed regions cropped from Fig. 17(a)–(f) are, respectively, shown in Fig. 18(a)–(f).

From Figs. 17 and 18, we can see that the resolution has certainly increased after using the SR technique compared with the results of the BI interpolated and the BCI interpolated results. Of the three SR methods, the U-curve method provides a clearer result than the other two, seen especially clearly from the detailed regions.

C. Optimal Analysis

To further show the efficacy of the U-curve, we plotted the change tendency of the MSE value versus the regularization parameter of the "cameraman" image in Case 1. The tendency

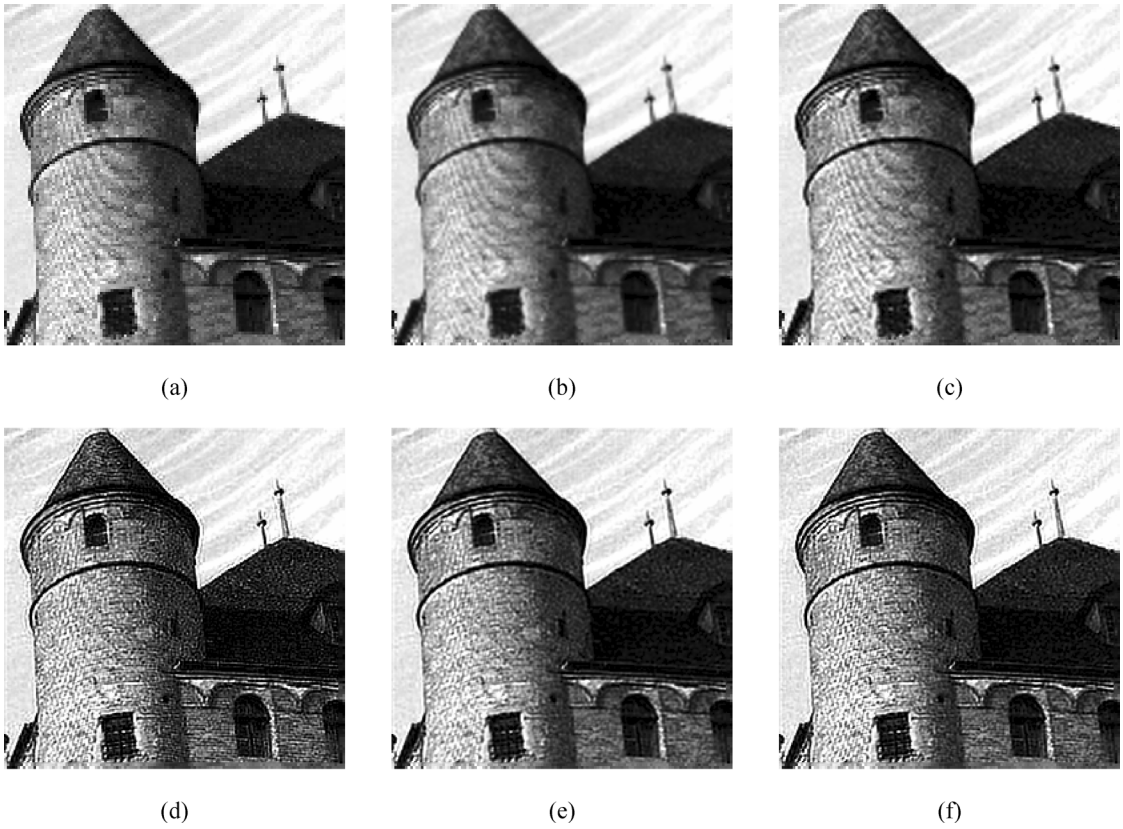

(a) (b) (c)

(d) (e) (f)

Fig. 15. Reconstruction results of the "castle" image. (a) LR image. (b) BI. (c) BCI. (d) Adaptive iteration. (e) L-curve. (f) U-curve.

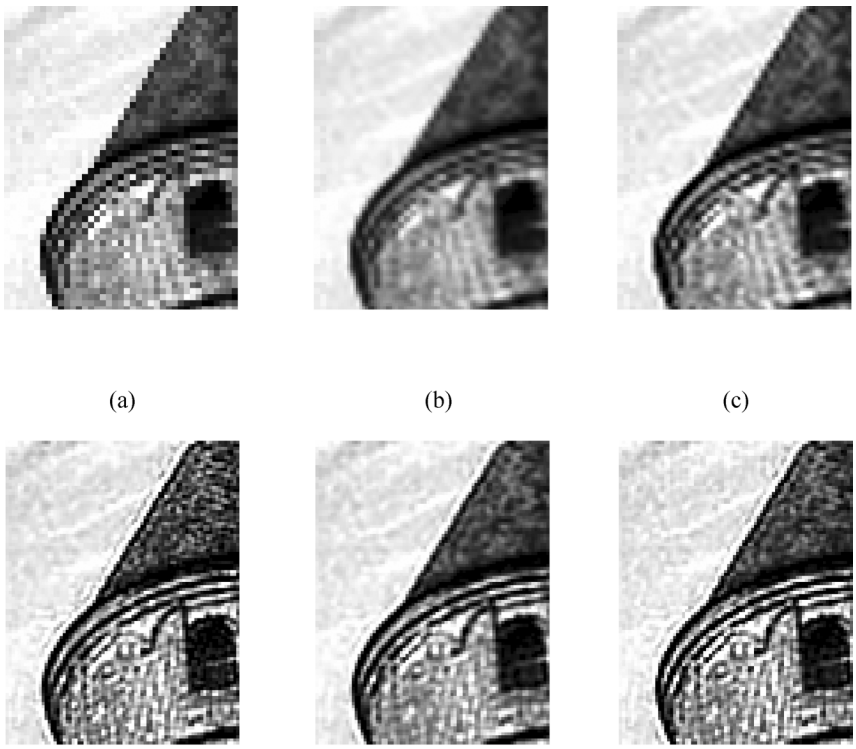

(a) (b) (c)

(d) (e) (f)

Fig. 16. Detailed regions cropped from Fig. 15. (a) LR image. (b) BI. (c) BCI. (d) Adaptive iteration. (e) L-curve. (f) U-curve.

Fig. 17. Reconstruction results of the "text" image. (a) LR image. (b) BI. (c) BCI. (d) Adaptive iteration. (e) L-curve. (f) U-curve.

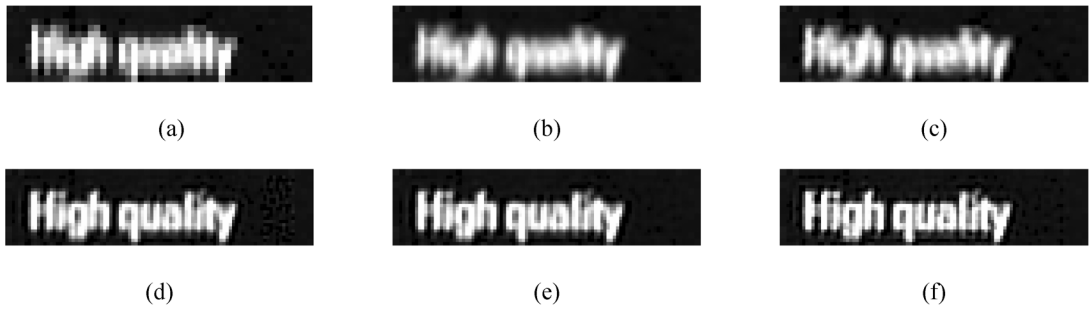

Fig. 18. Detailed regions cropped from Fig. 17. (a) LR image. (b) BI. (c) BCI. (d) Adaptive iteration. (e) L-curve. (f) U-curve.

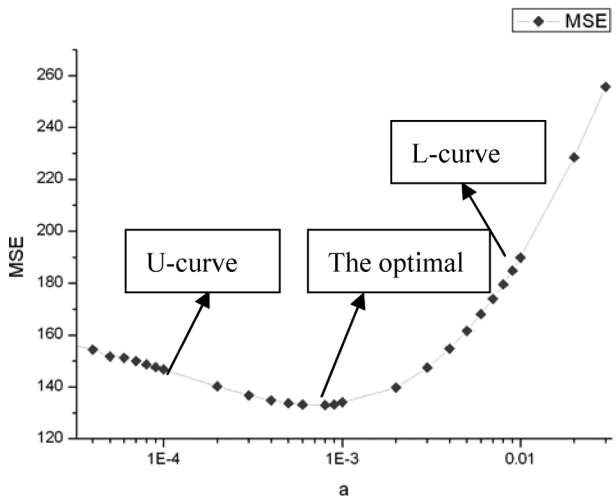

Fig. 19. Change of the MSE value versus the regularization parameter.

line is shown in Fig. 19. It can be clearly seen that the U-curve method provides a more accurate regularization parameter than the L-curve, and the selection parameter is closer to the optimal point.

VI. Conclusion

In this paper, a U-curve method is utilized to select the regularization parameter in the MAP SR reconstruction model. Firstly, the data fidelity and the prior model are used to construct a function for the regularization parameter. Then this function is plotted, which is the U-curve. Lastly, the maximum curvature point close to the left vertical part of the U-curve is selected as the optimal regularization parameter. Some advantages of our work are the following. First, an interval where the optimal regularization parameter probably exists is defined by the U-curve, which can greatly raise computational efficiency. Second, the U-curve method selects a more optimal regularization parameter than the L-curve, obtaining a better reconstruction result than the adaptive iteration method and L-curve method, and the reconstruction result can retain its robustness and efficacy in blurred or noisy situations.

However, the U-curve method based upon the Tikhonov regularization reconstruction model can still be revised in some aspects. For instance, the regularization parameter selected by the U-curve method is a bit smaller than the optimal regularization parameter. Therefore, Our future research will focus on how to

remedy this and select a more accurate regularization parameter, before using the U-curve method with some edge-preserving prior models, such as the Huber-MRF [21], TV [44] and BTV [45] models.

REFERENCES

[1] A. J. Martin, A. I. Gotlieb, and R. M. Henkelman, "High-resolution MR imaging of human arteries," *J. Magn. Reson. Imag.*, vol. 5, no. 1, pp. 93–100, 1995.

[2] X. Huang, L. Zhang, and P. Li, "Classification and extraction of spatial features in Urban areas using high-resolution multispectral imagery," *IEEE Geosci. Remote Sens. Lett.*, vol. 4, no. 2, pp. 260–264, Apr. 2007.

[3] L. Zhang, H. Zhang, H. Shen, and P. Li, "A super-resolution reconstruction algorithm for surveillance images," *Signal Process.*, vol. 90, no. 3, pp. 848–859, 2010.

[4] R. Y. Tsai and T. S. Huang, "Multiple frame image restoration and registration," in *Advances in Computer Vision and Image Processing*. Greenwich, CT: JAI Press, 1984, pp. 317–339.

[5] S. P. Kim, N. K. Bose, and H. M. Valenzuela, "Recursive reconstruction of high resolution image from noisy undersampled multiframes," *IEEE Trans. Acoust., Speech, Signal Process.*, vol. 38, no. 6, pp. 1013–1027, Jun. 1990.

[6] S. P. Kim and W.-Y. Su, "Recursive high-resolution reconstruction of blurred multiframe images," *IEEE Trans. Image Proc.*, vol. 2, no. 4, pp. 534–539, Oct. 1993.

[7] N. K. Bose, H. C. Kim, and H. M. Valenzuela, "Recursive implementation of total least squares algorithm for image reconstruction from noisy, undersampled multiframes," in *Proc. IEEE Conf. Acoust., Speech Signal Process.*, Minneapolis, MN, Apr. 1993, vol. 5, pp. 269–272.

[8] S. Rhee and M. G. Kang, "Discrete cosine transform based regularized high-resolution image reconstruction algorithm," *Opt. Eng.*, vol. 38, no. 8, pp. 1348–1356, 1999.

[9] R. H. Chan, T. F. Chan, L. Shen, and Z. Shen, "Wavelet algorithms for high-resolution image reconstruction," *SIAM J. Sci. Comput.*, vol. 24, no. 4, pp. 1408–1432, 2003.

[10] M. K. Ng, C. K. Sze, and S. P. Yung, "Wavelet algorithms for deblurring models," *Int. J. Imag. Syst. Technol.*, vol. 14, no. 3, pp. 113–121, 2004.

[11] N. Nguyen and P. Milanfar, "A wavelet-based interpolation restoration method for superresolution (wavelet superresolution)," *Circuits Syst. Signal Process.*, vol. 19, no. 4, pp. 321–338, 2000.

[12] H. Ji and C. Fermuller, "Robust wavelet-based super-resolution reconstruction: Theory and algorithm," *IEEE Trans. Pattern Anal. Mach. Intell.*, vol. 31, no. 4, pp. 649–660, Apr. 2009.

[13] H. Ur and D. Gross, "Improved resolution from sub-pixel shifted pictures," *CVGIP, Graph. Models Image Process.*, vol. 53, pp. 181–186, 1992.

[14] M. S. Alam, J. G. Bognar, R. C. Hardie, and B. J. Yasuda, "Infrared image registration and high-resolution reconstruction using multiple translationally shifted aliased video frames," *IEEE Trans. Instrum. Meas.*, vol. 49, no. 5, pp. 915–923, Oct. 2000.

[15] M. Irani and S. Peleg, "Improving resolution by image registration," *CVGIP, Graph. Models Image Process.*, vol. 53, pp. 231–239, 1991.

[16] M. Irani and S. Peleg, "Motion analysis for image enhancement resolution, occlusion, and transparency," *J. Vis. Commun. Image Represent.*, vol. 4, no. 4, pp. 324–335, 1993.

[17] H. Stark and P. Oskoui, "High resolution image recovery from image-plane arrays, using convex projections," *J. Opt. Soc. Amer. A*, vol. 6, pp. 1715–1726, 1989.

[18] A. J. Patti, M. I. Sezan, and A. M. Tekalp, "Super resolution video reconstruction with arbitrary sampling lattices and nonzero aperture time," *IEEE Trans. Image Process.*, vol. 6, no. 8, pp. 1064–1076, Aug. 1997.

[19] R. C. Hardie, K. J. Barnard, J. G. Bognar, E. E. Armstrong, and E. A. Watson, "High-resolution image reconstruction from a sequence of rotated and translated frames and its application to an infrared imaging system," *Opt. Eng.*, vol. 37, no. 1, pp. 247–260, 1998.

[20] B. C. Tom and A. K. Katsaggelos, "Reconstruction of a high-resolution image by simultaneous registration, restoration, and interpolation of low-resolution images," in *Proc. IEEE Int. Conf. Image Process.*, Washington, DC, 1995, vol. 2, pp. 539–542.

[21] R. R. Schulz and R. L. Stevenson, "Extraction of high-resolution frames from video sequences," *IEEE Trans. Image Process.*, vol. 5, no. 6, pp. 996–1011, Jun. 1996.

[22] R. C. Hardie, K. J. Barnard, and E. E. Armstrong, "Joint MAP registration and high-resolution image estimation using a sequence of undersampled images," *IEEE Trans. Image Process.*, vol. 6, no. 12, pp. 1621–1633, Dec. 1997.

[23] H. Shen, L. Zhang, B. Huang, and P. Li, "A MAP approach for joint motion estimation, segmentation and super-resolution," *IEEE Trans. Image Process.*, vol. 16, no. 2, pp. 479–490, Feb. 2007.

[24] N. A. Woods, N. P. Galatsanos, and A. K. Katsaggelos, "Stochastic methods for joint registration, restoration, and interpolation of multiple undersampled images," *IEEE Trans. Image Process.*, vol. 15, no. 1, pp. 201–213, Jan. 2006.

[25] M. Elad and A. Feuer, "Restoration of a single superresolution image from several blurred, noisy, and undersampled measured images," *IEEE Trans. Image Process.*, vol. 6, no. 12, pp. 1646–1658, Dec. 1997.

[26] S. Farsiu, M. Elad, and P. Milanfar, "Multiframe demosaicing and super-resolution of color images," *IEEE Trans. Image Process.*, vol. 15, no. 1, pp. 141–159, Jan. 2006.

[27] T. Akgun, Y. Altunbasak, and R. M. Mersereau, "Superresolution reconstruction of hyperspectral images," *IEEE Trans. Image Process.*, vol. 14, no. 11, pp. 1860–1875, Nov. 2005.

[28] H. Shen, M. K. Ng, P. Li, and L. Zhang, "Super-resolution reconstruction algorithm to MODIS remote sensing images," *Comput. J.*, vol. 52, no. 1, pp. 90–100, 2009.

[29] M. Vega, J. Mateos, R. Molina, and A. K. Katsaggelos, "Super-resolution of multispectral images," *Comput. J.*, vol. 52, no. 1, pp. 153–167, 2009.

[30] N. K. Bose, S. Lertrattanapanich, and J. Koo, "Advances in superresolution using L-curve," in *Proc. Int. Symp. Circuits Syst.*, 2001, vol. 2, pp. 433–436.

[31] C. L. Lawson and R. J. Hanson, *Solving Least Squares Problems*. Upper Saddle River, NJ: Prentice-Hall, 1974.

[32] P. C. Hansen and D. P. O'Leary, "The use of the L-curve in the regularization of discrete ill-posed problems," *SIAM J. Sci. Comput.*, vol. 14, no. 6, pp. 1487–1503, 1993.

[33] N. Nguyen, P. Milanfar, and G. Golub, "A computationally efficient superresolution image reconstruction algorithm," *IEEE Trans. Image Process.*, vol. 10, no. 4, pp. 573–583, Apr. 2001.

[34] G. Golub, M. Heath, and G. Wahba, "Generalized cross-validation as a method for choosing a good ridge parameter," *Technometrics*, vol. 21, pp. 215–223, 1979.

[35] M. G. Kang and A. K. Katsaggelos, "General choice of the regularization functional in regularized mage restoration," *IEEE Trans. Image Process.*, vol. 4, no. 5, pp. 594–602, May 1995.

[36] H. He and L. P. Kondi, "An image super-resolution algorithm for different error levels per frame," *IEEE Trans. Image Process.*, vol. 15, no. 3, pp. 592–603, Mar. 2006.

[37] R. Molina, M. Vega, J. Abad, and A. K. Katsaggelos, "Parameter estimation in Bayesian high-resolution image reconstruction with multisensors," *IEEE Trans. Image Process.*, vol. 12, no. 12, pp. 1655–1667, Dec. 2003.

[38] M. V. W. Zibetti, F. S. V. Baz'an, and J. Mayer, "Determining the regularization parameters for super-resolution problems," *Signal Process.*, vol. 88, no. 12, pp. 2890–2901, 2008.

[39] D. Krawczy-Stando and M. Rudnicki, "Regularization parameter selection in discrete-ill posed problems—The use of the U-curve," *Int. J. Appl. Math. Comput. Sci.*, vol. 2, no. 17, pp. 157–164, 2007.

[40] Z. Wang, A. C. Bovik, and H. R. Sheikh, "Image quality assessment: From error visibility to structural similarity," *IEEE Trans. Image Process.*, vol. 13, no. 4, pp. 600–612, Apr. 2004.

[41] EPFL, EPFL Software [Online]. Available: http://lcavwww.epfl.ch/software/superresolution/index.html

[42] University of California, Santa Cruz, Milanfar Software [Online]. Available: http://users.soe.ucsc.edu/~milanfar/software/sr-datasets.html

[43] P. Vandewalle, S. Susstrunk, and M. Vetterli, "A frequency domain approach to registration of aliased images with application to super-resolution," *EURASIP J. Appl. Signal Process.*, pp. 1–14, 2006.

[44] M. K. Ng, H. Shen, E. Y. Lam, and L. Zhang, "A total variation regularization based super-resolution reconstruction algorithm for digital video," *EURASIP J. Adv. Signal Process.*, pp. 1–16, 2007.

[45] S. Farsiu, M. D. Robinson, M. Elad, and P. Milanfar, "Fast and robust multiframe super-resolution," *IEEE Trans. Image Process.*, vol. 13, no. 10, pp. 1327–1344, Oct. 2004.

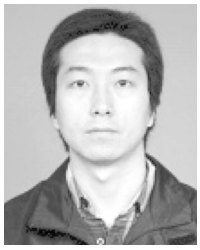

Qiangqiang Yuan received the B.S. degree in surveying and mapping engineering from Wuhan University, Wuhan, China, in 2006, where he is currently pursuing the Ph.D. degree at the State Key Laboratory of Information Engineering in Surveying, Mapping and Remote Sensing.

His current research interests focus on image restoration, super-resolution, and remote sensing image enhancement.

Liangpei Zhang received the B.S. degree in physics from Hunan Normal University, ChangSha, China, in 1982, the M.S. degree in optics from the Xi'anInstitute of Optics and Precision Mechanics, Chinese Academy of Sciences, Xi'an, China, in 1988, and the Ph.D. degree in photogrammetry and remote sensing from Wuhan University, Wuhan, China, in 1998.

He is currently with the State Key Laboratory of Information Engineering in Surveying, Mapping and Remote Sensing, Wuhan University, as the Head of the Remote Sensing Division. He is also a "Chang-Jiang Scholar" Chair Professor appointed by the Ministry of Education, China. He has more than 180 research papers and five patents. His research interests include hyperspectral remote sensing, high-resolution remote sensing, image processing, and artificial intelligence.

Dr. Zhang is a Fellow of Institution of Electrical Engineers, Executive Member (Board of Governor) of the China National Committee of International Geosphere-Biosphere Program, Executive Member for the China Society of Image and Graphics, and others. He regularly serves as a Cochair of the series SPIE Conferences on Multispectral Image Processing and Pattern Recognition, Conference on Asia Remote Sensing, and many other conferences. He edits several conference proceedings, issues, and the Geoinformatics Symposiums. He also serves as an Associate Editor of the *International Journal of Ambient Computing and Intelligence*, *International Journal of Image and Graphics*, *Journal of Geo-spatial Information Science*, and the *Journal of Remote Sensing*.

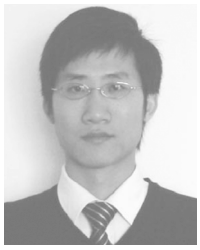

Huanfeng Shen received the B.S. degree in surveying and mapping engineering and the Ph.D. degree in photogrammetry and remote sensing from Wuhan University, Wuhan, China, in 2002 and 2007, respectively.

Since 2007, he has been an Associate Professor with the School of Resource and Environmental Science, Wuhan University,. His current research interests focus on image reconstruction and remote sensing image processing and application.

Pingxiang Li received the B.S., M.S., and Ph.D. degrees in photogrammetry and remote sensing from Wuhan University, Wuhan, China, in 1986, 1994, and 2003, respectively.

Since 2002, he has been a Professor with the State Key Laboratory of Information Engineering in Surveying, Mapping, and Remote Sensing, Wuhan University. His research interests include photogrammetry and SAR image processing.